Evaluating Analog Self-Interference Cancellation for In-Band Full-Duplex Wireless Communication

Jonathan Shilling and Chao Chen*

Department of Electrical and Computer Engineering, Purdue University Fort Wayne, Indiana 46805, USA
*Correspondence: chenc@pfw.edu

***Abstract*—In-band full-duplex (IBFD) technology allows simultaneous transmission and reception in the same frequency band to boost spectral efficiency. However, self-interference, introduced by transmitter-to-receiver leakage, poses the biggest obstacle to the realization of IBFD. Altogether IBFD radio performance and effective network throughput are directly correlated with the amount of energy suppressed by self-interference cancellation (SIC). In this work a model of an IBFD transceiver, featuring an adaptive, analog-domain, tapped-branch self-interference canceller, was developed to evaluate the inimical effects attributable to the various noise and nonlinear distortions of the simulated transceiver components. Results of the simulation show that noise incursions and nonlinearity in the transmission channel produced a negligible effect on the overall cancellation performance. However, the effectiveness of the cancellation hardware is highly dependent on the level of intrinsic nonlinearity within the canceller's own components. Consideration of these non-ideal characteristics should be an essential part of analog SIC design to prevent any intrinsic limitations on the cancellation performance.**

***Keywords*—in-band full-duplex, analog self-interference cancellation, nonlinearity**

I. Introduction

The revolution of wireless technology has led to the creation of a vast network of wireless devices that are essential to our daily lives and the productivity of the society. However, this increased demand for wireless services has put a strain on the limited wireless spectrum, making it necessary to find ways to increase bandwidth, channel capacity, and access rates. Long-Term Evolution (LTE) wireless networks, existing 5G technologies, and developing 6G networks, have highlighted the need for careful and efficient spectrum utilization strategies. One of these promising techniques to improve spectrum efficiency is in-band full-duplex (IBFD) operation. A long-standing principle of communication states that for successful communication, transceivers that are using the same physical medium must transmit and receive data in either non-contiguous timeslots of non-overlapping frequency bands [1]. IBFD defiantly challenges this belief by allowing simultaneous, identical spectrum transmission and reception. By doing this, IBFD has the potential to double the spectral efficiency from its half-duplex counterpart. Some other potential benefits of IBFD include increased capacity, decreased outage probability, reduced end-to-end delay, and improved quality of service for wireless networks [2-4]. It has also been suggested that IBFD technologies may provide additional security benefits [5, 6]. Additionally, IBFD could allow for more flexible and efficient use of the wireless spectrum, potentially enabling the development of new types of wireless services and applications. For example, one possible application of IBFD is using simultaneous transmission and scanning at a secondary user to improve detection quality in cognitive radio environments [7].

In spite that multiple small-scale IBFD radio prototypes have been built [8-10], there are still outstanding impediments to the viability of larger-scale IBFD networks. Some of the main obstacles include the need for efficient full-duplex aware MAC protocols, the potential increase in power consumption and its impact on existing mobile communication standards, and lack of effective and adaptive self-interference cancellation technologies [11]. The biggest obstacle to the implementation of IBFD networks is the self-interfering environment in these transceivers. Self-interference (SI) occurs when a transceiver's transmission interferes with its own ability to receive the intended signal in the same frequency band. This interfering signal "leaks" into the reception path, often at a much higher power level than the desired signal, and causes amplifier saturation and reduced sensitivity of the ADC's dynamic range. According to [4], effective self-interference cancellation (SIC) for IBFD transceivers must be able to suppress SI to the level of the receiver's noise floor, which requires a suppression capability on the order of 110dB or greater. In order to achieve such high levels, it is imperative to use multiple different cancellation mechanisms. Self-interference cancellation techniques are often employed in domains classified as propagation, analog, or digital [12]. Among these, the greatest degree of SI cancellation is often achieved in the analog-domain, with the goal of eliminating the as much as possible of the interfering signal before it reaches the receiver's ADC. Furthermore, the quality of analog domain cancellation has a direct impact on the success of the proceeding SIC in the digital domain [13]. Therefore, the primary mode of cancellation in an IBFD system is often in the analog domain.

Manuscript received August 20, 2022; revised October 20, 2022; accepted December 28, 2022.

doi:10.12720/jcm.18.4.256-266

Though fundamentally SIC is often described in terms of a simple subtractive operation, in practice it proves to be not as simple since the transmitted signal often undergoes a conversion to an IF analog frequency before up-conversion to a higher RF carrier frequency. These operations can, and often inevitably do, impart distortions along the way. Hence, SI can no longer be reliably and accurately anticipated from the baseband signal without further assumed knowledge. Distortion may be ascribed to a myriad of causations including quantization noise, power amplifier (PA) nonlinearity, phase noise, in-phase and quadrature-phase (I/Q) imbalance, circulator leakage, and system discontinuities (e.g., antenna reflection). All of the aforementioned aspects are likely to affect SIC and result in non-ideal cancellation in the receiving path. In turn, overall degradation in system functionality results. The implications of this forecast increased difficulty in mitigating SI as the desire for ever higher data rates spurs an increase in the complexity of an RF front end with inclusion of new technologies like carrier aggregation, higher-order modulation, and multiple-input multiple-output (MIMO) techniques [14].

This study focuses on a technique of active analog cancellation; a method of subtractive SIC in the reception path prior to conversion back to the digital baseband. Most current models of SI cancellation [15] fail to consider for nonlinearity and noise imparted by the SI canceller in the receive circuitry, as an unintentional consequence of the hardware design. In this work, we investigate the sources of noisy incursions and nonlinearities attributable to both the IBFD transmission route and the analog SIC hardware. We also examine how these adversarial effects can degrade the overall system SIC performance. Specifically, in MATLAB, we implemented a modular design of a 512 state QAM IBFD transceiver. This model includes several significant sources of adverse impact, such as Nyquist-Johnson thermal noise, oscillator phase noise, transient power supply perturbations, amplifier harmonics, and RF mixer harmonics and intermodulation distortion products. The transceiver model includes an analog SIC hardware architecture that is implemented as a parallel-branched analog canceller. This canceller samples the transmission signal after it has been affected by noise and nonlinear distortion. Using a gradient descent algorithm, a viable real-time method is employed to dynamically determined each branches phase and attenuation values in the SIC mechanism. The SIC system performance is evaluated by observing the amount of distortion it is able to mitigate. Through our study, we found that 60dB of cancellation can be achieved through the analog SIC. However, the cancellation capability is heavily dependent on its own level of nonlinearity. Specifically, degradation of 35dB is observed in the cancellation performance as distortions particular to the cancellation rose from -80dBm baseline levels to worst case -10dBm levels. These initial results imply that it is important to carefully consider the inimical effects of unwanted signal products when designing and implementing analog SIC hardware.

The rest of this paper is organized as follows: Section II summarizes the related work. Section III explores the main sources of noise and nonlinearity in the IBFD transceiver, along with the mathematical models to characterize them. Section IV presents our IBFD transceiver model, its major nonlinear components, and the analog SIC hardware architecture. The method to evaluate the SIC performance is also explained. Section V summarizes the results in evaluating the SIC performance of the IBFD transceiver. Finally, Section VI concludes our work and discusses potential directions for future research.

II. Related Work

One of the first notable IBFD wireless systems was designed by researchers at Stanford University in 2010 [8]. This system was built utilizing off-the-shelf IEEE 802.15.4 hardware with software-defined radios. IBFD communications were implemented with all three ways of interference cancellation. In propagation domain, antenna cancellation was achieved by placing two antennae at a distance of d and $d+\lambda/2$ from the receiver antenna, creating a null region against the SI signal. In addition, active analog cancellation was done using a Renesas QHx220 Interference Canceller IC, which provided about 20dB of isolation. For digital cancellation, a technique called coherent detection was used, which allows for the isolation of the conflated SI signal. Testing results showed a SIC of $\geq$60dB and a throughput gain of 84% of comparative half-duplex operation [8]. Overall, the authors concluded that the methodology was effective within the constraints of the system, but the isolation achieved was limited to 80dB, which was likely insufficient. They also noted that the antenna cancellation method was only effective for narrowband signals.

Another early IBFD system was built at Rice University also in 2010. The researchers utilized off-the-shelf WARPLab 2.4GHz radios to design an IBFD system that yielded around 80dB of Tx-to-Rx isolation [9]. Propagation domain suppression was achieved with a conventional bistatic antenna configuration. Active analog cancellation was implemented via a deconstructive addition in the receiver path, whereas digital cancellation was handled through offline processing in MATLAB. Measurement results and calculations showed significant improvement in terms of achievable rate per frame in the IBFD scenario compared with its half-duplex counterpart.

In 2013, researchers at Stanford University presented the first functional IEEE 802.11ac compliant full-duplex system [10]. This system utilized a hybrid cancellation scheme to provide 110dB of SIC in a noisy indoor environment. Importantly, the authors of this study argued that given a transmitter with a power level of 20dBm and a receiver noise floor of -90dB, their IBFD system would require at least 110dB of linear SIC of the main signal in order to function properly. Additionally, the system would need to achieve 80dB of non-linear component SIC and 50dB of transmitter noise cancellation in order to be effective. In the analog domain, their hardware implementation consisted of a canceller with a fixed delay line and variable attenuator that was fed a tapped version of the transmission signal. Their digital approach used the knowledge of a message's preamble to develop a linear and

nonlinear model. The novel aspects of their work include their interpretation of the problem and the tuning algorithms used. They showed that by positioning the actual delay experienced by the SI signal within the sinc interpolation function, it was possible to transform attenuation weight estimation into a frequency-domain problem of sampling and interpolation. To further boost cancellation in the digital domain, they modeled the anticipated SI as a non-causal function and used samples from future instances of the preamble packet to converge on the present SI. This approach relied on the availability of the entire preamble packet. Finally, they managed additional nonlinear cancellation in the digital domain by modelling expected nonlinear components as a simple Taylor Series expansion. To minimize the number of unknown variables needed to be solved for, they empirically determined which variables were ineffective and omitted them from the model. Using a SMBV 100A signal generator as a transmitter and a Rohde & Schwarz spectrum analyzer as a receiver substitute, the researchers were able to show a cancellation capability of ≥110dB at a throughput gain of 1.87 times that of half-duplex operation with the above-mentioned techniques [10].

In recent years, there have been increased efforts in developing techniques in removing self-interference to further IBFD technology. In the digital domain, extensive progress has been made to create more effective memory-inclusive nonlinear models, such as the parallel Hammerstein model, the Wiener-Hammerstein model, and other Volterra derivative models [13]. Other techniques that have been explored include both transmit and receive beamforming, with the latter showing particular interest in MIMO applications where SI can be suppressed by adaptively adjusting the individual antenna weights according to the current SI channel's conditions [16]. In addition to physical layer SIC techniques, efficient and effective technologies at the MAC layer have also been studied. The aim has typically been to develop IBFD-conducive protocols that minimize power consumption, maintain legacy compatibility, and address inefficiencies resulting from anticipated traffic asymmetry [17, 18].

III. Noise Analysis and Modeling

We start by exploring several major sources of noise and nonlinearity that occurs in standard transceiver hardware. The mathematical models and characteristic considerations are presented. These models will be incorporated in the IBFD transceiver model in Section IV.

A. Johnson-Nyquist Noise

Johnson-Nyquist noise refers to the thermal noise that is inherently present in all materials, regardless of material type or circuit functionality, due to the thermal movement of charge carriers. Thermal agitation of charge carriers causes minute perturbation in current and charge density. Hence, minor alterations in associated electric and magnetic fields manifest as bandlimited white noise [19]. Under ordinary thermal circumstances, Johnson-Nyquist noise can be characterized by a noise power, N, calculated by:

$$N = k_B T B, \tag{1}$$

where k_B is the Boltzmann constant ($1.38 \cdot 10^{-23} JK^{-1}$), B the bandwidth (Hz), and T the temperature (Kelvin), [20]. As a result of the thermal agitation, given a nominal resistance, R_o, the system's voltage is calculable from:

$$v_{TN} = \sqrt{2 k_B T B R_o}. \tag{2}$$

Values used in our simulation were 218.15 Kelvin, 50Ω, and 1 Hz for temperature, resistance, and bandwidth, respectively.

B. Oscillator Phase Noise

An electronic oscillator aims to generate a sinusoidal waveform with a single specified frequency. In practice, electronic oscillators are non-linear in nature with associate output spectrum typically contaminated with undesired energy components. This noise is often described in terms of an offset frequency from the ideal oscillation and caused by minute phase fluctuations, $\vartheta(t)$. This noise is typically characterized using its single sideband power spectral density (PSD) and written as $\mathcal{L}(f) = \frac{S_\vartheta(f)}{2}$. Here the PSD of the phase fluctuations is denoted by $S_\vartheta(f)$. A phase noise profile typical of a low-phase noise oscillator is depicted in Table I. This profile provides detailed information about the phase noise characteristics of the oscillator.

TABLE I: Simulated Oscillator Phase Noise Profile

Frequency Offset (Hz)	Phase Noise (dBc/Hz)
10	-70
100	-100
1,000	-125
10,000	-145
100,000	-160
1,000,000	-169
10,000,000	-170

C. Nonlinearity

This research considers simulations and cases that are modeled in a transitory discrete-event manner. As a result, the need for memory inclusion is not necessary. In addition, a static polynomial model was found to have similar or better performance in terms of the model error in RF PAs compared to more complex memory models [21]. As a result, Taylor series expansion is used to evaluate the distortion of the nonlinear devices, such as mixers and PAs, in our IBFD transceiver model. In particular, the Taylor series expansion of the output $v_o(t)$, given an input $v_i(t)$, can be expressed as:

$$v_o(t) = \sum_{k=0}^{N} a_k v_i^k(t), \tag{3}$$

where N is the order and a_k is a scalar coefficient.

Assuming a 5th-order and simple sinusoidal input waveform of $A cos\omega t$, Eq. (3), expansion, simplification, and further reduction will result in an output spectrum composed of the first 5 harmonics. This spectrum, in terms of coefficients, is detailed in Table II. In this case, the nonlinear device behaves as a harmonic generator. This function effectively models single-input nonlinear devices,

such as power and low-noise amplifiers (LNA), that do not exhibit significant intermodulation distortion.

TABLE II: COEFFICIENTS FOR 5TH-ORDER HARMONIC EXPANSION

Spectral Component	Coefficient
DC	$a_0 + a_2A^2/2 + 3a_4A^4/8$
ω	$a_1A + 3a_3A^3/4 + 5a_5A^4/8$
2ω	$a_2A^2/2 + a_4A^4/4$
3ω	$a_3A^3/2 + 5a_5A^5/8$
4ω	$a_4A^4/8$
5ω	$a_5A^5/16$

For other nonlinear devices that pass through more than one frequency inputs, intermodulation distortion (IMD) may present. Such application cases include RF mixers as well as situations where extraneous signal intrusion presents in a semiconductor device, *e.g.*, clock mixing with D/A or A/D conversion. In these cases, a nonlinear model with an additive two-tone input can be useful for analyzing the behavior of the device. Commonly, intermodulation distortion products may only be characterized by a device manufacturer up to the 3rd product. Viewing a 3rd-order nonlinear product Eq. (3) and an input with two coupled signals, i.e., $v_i(t) = A_1 cos\omega_1 t + A_2 cos\omega_2 t$, a generated output spectrum with the harmonics for each individual frequency, as well as the nonlinear interaction of a two-tone system is produced (i.e., both 2nd- and 3rd-order IMD products). These can be found listed in Table III. It is clear that both the original multiplicative factors (a_1, a_2, a_3 ...) of the nonlinear model and the input amplitudes (A_1 and A_2) determine the magnitude of each spectral component.

TABLE III: COEFFICIENTS FOR 3RD-ORDER EXPANSION WITH INTERMODULATION DISTORTION

Spectral Component(s)	Coefficient
DC	$a_0 + a_2(A_1^2 + A_2^2)/2$
ω_1	$a_1A_1 + 3a_3(A_1^3 + 2A_1A_2^2)/4$
ω_2	$a_1A_2 + 3a_3(A_2^3 + 2A_1^2A_2)/4$
$2\omega_1$	$a_2A_1^2/2$
$2\omega_2$	$a_2A_2^2/2$
$3\omega_1$	$a_3A_1^3/4$
$3\omega_2$	$a_3A_2^3/4$
$\omega_2 \pm \omega_1$	$a_2A_1A_2$
$2\omega_1 \pm \omega_2$	$3a_3A_1^2A_2/4$
$2\omega_2 \pm \omega_1$	$3a_3A_1A_2^2/4$

Two particular IMD products that are often mentioned in amplifier and mixer datasheets are the second-order intercept (IP2) and the third-order intercept points (IP3). These points are considered especially harmful due to the fact that if ω_1 and ω_2 are relatively close, then $2\omega_1 - \omega_2$ and $2\omega_2 - \omega_1$ will fall spectrally close to the ideal amplifier outputs ω_1 and ω_2, and $2\omega_1$ and $2\omega_2$ are very close to the ideal mixer summation output $\omega_1 + \omega_2$.

IV. IBFD TRANSCEIVER SIMULATION MODEL

Evaluation of SIC using the analog domain methodology presented, with the presence of noisy and nonlinear components, is done by programmatically using an aggregated component model of an IBFD transceiver in MATLAB. The most egregious noise sources introduced in Section III are included in this model.

A. Overview of Transceiver Architecture

Our IBFD architecture model, featuring a QAM scheme, is shown in Fig. 1. The system's input is a pseudo-random bit sequence (PRBS) pattern of order 31. Equivalently in I and Q transmission channels, the digitized baseband PRBS sequence undergoes analog conversion before modulation onto a higher frequency RF carrier. After mixing, both I/Q signals pass through an RF PA before being transmitted through the duplexer and the antenna.

Functionality in the receiving channel mirrors that of the transmission path in a corresponding manner in order to facilitate appropriate demodulation of an anticipated QAM signal. The received signal has a lower power level but is accompanied by a much stronger SI component because of self-interference from the transmission path. Possible sources of the self-interference include:

(i) Finite component isolation leading to Tx-Rx leakage in the circulator/duplexer.
(ii) Partial energy reflection due to discontinuity between transceiver and antenna (i.e., impedance mismatch).
(iii) Ambient "bounce-back" of transmitted EM waves (i.e., environmental reflections).

Post reception, the transceiver attempts to maximize SI cancellation using the subtractive analog domain technique presented prior to any amplification. This technique extracts its cancellation signal by syphoning a portion of the Tx signal immediately post PA in the Tx channel. Extraction at this site affords implicit inclusion of all transmission noise and nonlinear incursions (i.e., additional modeling of auxiliary Tx paths is unneeded). However, this approach may increase SI canceling and associated circuitry complexity in the RF band and MIMO applications [22]. Subsequently, residual SI and the signal-of-interest (SOI) travel through the Rx LNA that ideally features a higher ameliorating dynamic range for the non-ideal SIC. From here, the SOI with remaining SI undergoes baseband demodulation and digitization by the ADC. At this point, subsequent digital domain SIC could be employed. Referring to the de facto calculated SI cancellation target of 110dB [10], an analog target of an estimated 60dB of cancellation is likely.

B. Digital-to-Analog Converter

The ideal input-to-output relationship of a digital-to-analog convertor (DAC) is:

$$v_{DAC} = \frac{D(v_{ref} - v_d)}{2^b - 1}, \quad (4)$$

where the equivalent input decimal value, reference voltage, and inherent voltage drop are denoted by D, v_{ref}, and v_d, respectively. The DAC's bit depth is denoted by b. Both transceiver DACs in corresponding I/Q sections are simulated as nonlinear components with varying reference voltage affected outputs. In this simulation voltage drop and bit depth were set at 0.3V and 8 bits, respectively. v_{ref} is simulated in a means that each value is chosen in a probabilistic fashion corresponding to a normal distribution with mean of 1V and a variance set by the user.

Another main cause of noise considered in the DAC is non-ideal isolation with the clocking signal impinging (i.e., mixing) with the DAC's output. The simulations magnitude for the DAC's level of clock intrusion, CLK_{iso}, is set to -60dB. Nonlinear coefficients determining the severity of distortion components is calculated from the spurious free dynamic range (SFDR), which defines the difference between ideal spectral element's energy against that of the strongest spurious signal.

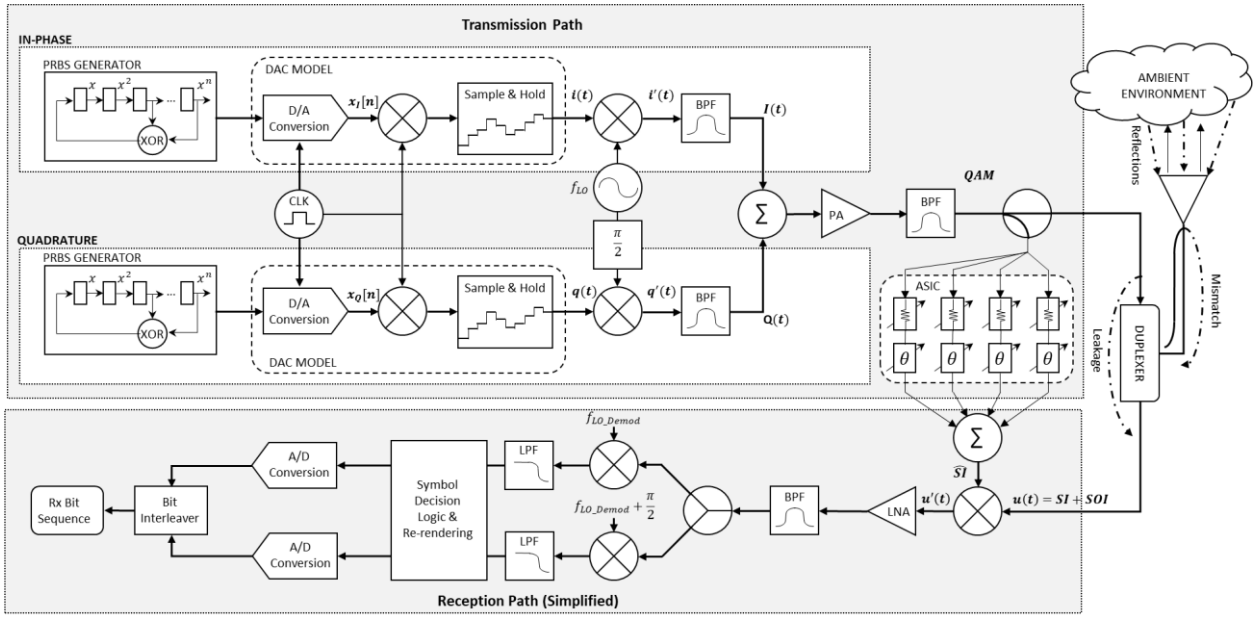

Figure 1. IBFD QAM transceiver architecture.

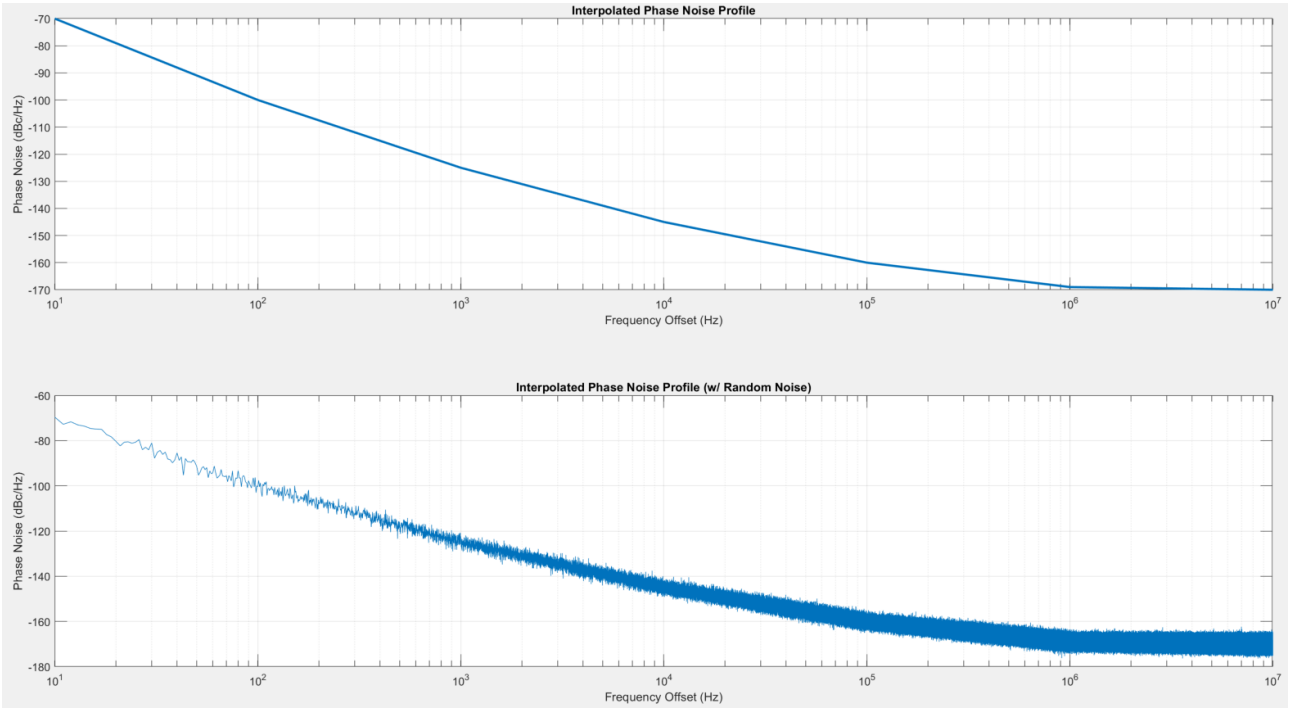

Figure 2. Phase noise profiles: piece-wise straight-line interpolation (top) and its noisy counterpart (bottom).

Following this, the noise spectral density (NSD) and transceiver Johnson-Nyquist noise spectrums are incorporated. Because of real-world non-ideal signal interpolation often observed in conversion circuitry, an emulated sample-and-hold component is incorporated. Note that many DAC's NSD profile's variance is only a few dB in the characterized spectrum. Therefore, the choice was made to treat the NSD affect as a bandlimited white noise. The decibel Gaussian white noise (additive) can be approximated according to:

$$NSD - 10\log_{10}\left(v_{ref} - v_d\right)^2/R, \quad (5)$$

Our simulation defined NSD at a value of -162dBc/Hz.

C. Phase-Noise Affected Oscillator

The DAC's unmodulated signal undergoes up-conversion by means of nonlinear mixing with the local oscillator. As mentioned in Section III-B, the presence of phase noise in the local oscillator can affect the performance of the transceiver. We use a two-phase process to create a plausible simulation phase noise spectrum. First, the frequency-noise level pairings defined in Table I are used to establish a baseline reference profile via interpolation to establish a piece-wise continuous spectrum. Next, a noise profile following a Gaussian distribution is generated and incorporated to emulate a stochastic nature in the overall phase noise profile. Fig. 2 displays a typical resultant phase noise profile that was generated during one run. The standard deviation in this was set at 2.1dBc.

Calculation of the voltage due to the phase noise approximated response was found using the formula:

$$v_{PN}(f) = \sqrt{2P_c Z_o \cdot 10^{\frac{dBc(f)}{10}}}, \quad (6)$$

Here P_c and Z_o represent the power (in watts) in the carrier and nominal impedance of the device, respectively. Then it follows that the phase noise, $\hat{\vartheta}(t)$, may be approximated using the relationship:

$$\hat{\vartheta}(t) = sin^{-1}\left(\int_{f_{start}}^{f_{end}} v_{PN}(f)\sin(2\pi f t)\, df\right). \quad (7)$$

In our simulations, an offset frequency spectrum spanning 10Hz to 10MHz was adopted with an output power of 9dBm. A characteristic impedance of 50Ω was used.

Note that in its discrete form, the integration in Eq. (7) is calculated as the summation of the term $v_{PN}(f)\sin(2\pi f t)$ at sampled frequencies in the specified range. However, as the phase-noise frequency range is wide, this method is computationally intensive. In practice, we decided to directly calculate only the phase noise at the most critical offset frequencies from 10Hz to 1KHz. For phase noise sections above 1KHz, weighted average of $v_{PN}(f)$ values at a median frequency in a corresponding section is used to ease the calculation.

D. RF Mixer and Bandpass Filter

Diodes and transistors are two commonly incorporated components used to facilitate mixing in RF mixers. Due to the semiconductor nature of these devices, they inherently contain nonlinear characteristics. For this reason, it was decided to treat all mixers as non-ideal devices with nonlinearity modelled as a third order Taylor series polynomial. The DC component (a_0) is set to its ideal value of 0 and the remaining three coefficients (a_1, a_2, a_3) are randomly set with a uniform distribution $U(0,1)$.

After the RF mixers, isolation of the wanted frequency components is achieved via a bandpass filter (BPF). In this way undesired second and third order intermodulation products may effectively be rejected both below and above the desired spectral elements. Simulation values set for the FIR BPF were chosen to have a roll-off factor and out of band rejection of 0.8 and -60dB, respectively. The desired spectral content ranged from $f_{LO} - f_{BBMax}$ to $f_{LO} + f_{BBMax}$, with the local oscillation frequency of 2.4GHz. The baseband bandwidth, f_{BBMax}, was set to 100MHz. Subsequently, the I and Q components predominantly subsume the wanted linear mixing products.

E. Power Amplifier

To generate the desired QAM signal the BPF *I* and *Q* components undergo another proceeding mixing stage. Again, this mixing is assumed to be done through a nonlinear device and is similarly modeled using a third order Taylor series polynomial. The susceptibility to I/Q imbalance is also implicitly incorporated in this stage, since any noisy, stochastic element from previous operations (*e.g.*, amplitude or phase variation) will effectively produce a non-ideal symbol level.

Following generation, the final stage of modification the QAM signal encounters before transmission is that of a PA. Again, with the semiconductor nature inherent to common PA designs, this stage is treated as nonlinear with fifth order polynomial representation. However, whereas two-tone IMD products were a predominant concern in the mixing stages, the PAs distortion is predominantly harmonic in type.

Using gain and IP3 values obtained from common off-the-shelf PA datasheets, the subsequent mathematical relationship was derived to approximate the voltage level of a feasible third order distortion product:

$$v_{IMD}^3 = \sqrt{10^{0.006{V_i}^2 - 2.42374} \cdot R}, \quad (8)$$

Here, v_{IMD}^3 denotes the third order voltage given an input, V_i and impedance, *R.* From (8), coefficients corresponding to Table III values were calculated and assigned to ensure realistic approximation. To incorporate a more stochastic model behavior, most of the simulations were allowed to have final values assigned from a Gaussian distribution centered around calculated value or allowed assignment from a uniform distribution $U(0,1)$. This allowed for broader exploration into the affective nature of these distortions.

In the simulation, incorporation of the transceiver's noise figure (NF) occurs post PA and is most overtly seen as a degradation in the noise floor. In other words, an increase in the bandlimited white noise content. Lastly, prior to SI canceller sampling and transmission, the transmission signal undergoes one final stage of an FIR BPF to again reject undesired nonlinear content.

F. Analog Self-Interference Canceller

Fig. 1 depicts the analog SIC architecture that employed a network of parallel branches each consisting of individually adjustable attenuation weights and phase shifts. Each tap uses real-time gradient descent optimization to find the best weight settings for its amplitude and phase. When all the taps are combined, the resulting signal $\widehat{SI}$ can be subtracted from the adulterated signal $u(t)$, ideally leaving the SOI for subsequent amplification. However, finite cancellation ultimately results in an output that consists of both SOI and residual

SI. This is denoted as $u'(t) = u(t) - \widehat{SI}$. After demodulation and digital conversion, further reduction of the residual SI can be achieved through digital domain cancellation. However, when evaluating the effectiveness of the analog cancellation, any proceeding digital cancellation becomes inconsequential. That is, no effect is observed on the analog cancellation. The signal $u'(t)$ is as far as we need to go in this evaluation. Therefore, in this study, all measurements and calculations are performed prior to the LNA amplification.

1) Amplitude and phase weights update

In our analog SIC, we used gradient descent algorithm to find the optimal tap attenuation and phase shift values that minimize $u'(t)$. Gradient descent is an optimization algorithm that works by iteratively moving in the direction of steepest descent, or the negative of the gradient. This process continues until the algorithm reaches a local or global minimum of the function [23]. Because analog cancellation typically does not assume any prior knowledge of the channel, a feedback mechanism is needed to effectively estimate the SI channel through the tapped parallel branches. Traditionally this was done using a transmitted training pilot-tone or preamble sequence. We also adopted this mechanism in our simulation runs: A small number of samples were used for training purposes before the transmission of the intended signal. These training samples allow the analog SIC circuit to adjust the tap weights using the gradient descent algorithm. Then the optimized tap weights were used during the transmission of remaining signals to measure the actual SIC performance.

Suppose an original signal is composed of an infinite series of sinusoidal harmonics, i.e., $x_1(t) = \sum_{i=1}^{\infty} a_i cos\omega_i t$. After that, some desired amplitude scaling α and phase shift θ are imparted to every component in this signal, resulting in $x_2(t) = \alpha \sum_{i=1}^{\infty} a_i \cos(\omega_i t + \theta)$. Using trigonometric identity, $x_2(t)$ can be rendered as:

$$\begin{aligned} x_2(t) &= \alpha \textstyle\sum_{i=1}^{\infty} a_i \cos\omega_i t cos\theta - a_i \sin\omega_i t sin\theta \\ &= \alpha cos\theta \textstyle\sum_{i=1}^{\infty} a_i \cos\omega_i t - \alpha sin\theta \sum_{i=1}^{\infty} a_i sin\omega_i t \\ &= \alpha(x_1(t) \cdot cos\theta - H\{x_1(t)\} \cdot sin\theta) \end{aligned} \quad (9)$$

where $H\{x_1(t)\}$ represents the Hilbert transform of our original aggregate signal $x_1(t)$. As the digitized samples extracted by the analog SIC for training represent a noise-affected multi-frequency discrete time series, Eq. (9) can be extended to its discrete form of:

$$\alpha x[n+\theta] \cong \alpha(x[n] \cdot \cos\theta - H\{x[n]\} \cdot \sin\theta). \quad (10)$$

In summary, the ideal time sequence $\alpha x(t+\theta)$ affected by path loss α and phase shift θ is estimated by the actual given discrete series $x[n]$ and its corresponding Hilbert transform, $H\{x[n]\}$. Multiplying the two by the cosine and sine of the desired phase shift, respectively, and then subtracting the two products effectively allows for phase shift incorporation for the entire spectral content of the discrete series. Subsequently, the multiplication by the amplitude weights renders overall signal attenuation by the specified amount. Assuming there is a total of N_{SI} paths that SI is coupled into the Rx channel, the SI signal in the jth Tx-Rx path can be represented by:

$$SI_j = \alpha_j\big(x[n] \cdot \cos\theta_j - H\{x[n]\} \cdot \sin\theta_j\big). \quad (11)$$

In this, the attenuation of the path and experienced phase shift are represented by α and θ, respectively.

Similarly, the modeled signal in the ith analog SIC branch, $\widehat{SI}_i$, after adjusting amplitude attenuation and phase shift, is determined to be:

$$\widehat{SI}_i = \beta_i(x[n] \cdot \cos\vartheta_i - H\{x[n]\} \cdot \sin\vartheta_i), \quad (12)$$

Here attenuation weight and phase shift values are denoted as β and ϑ, respectively.

Quantification of the effectiveness of the model is done by the mean-squared-error (MSE) between $\widehat{SI}$ and SI, where $\widehat{SI} = \sum_{i=1}^{N_{SIC}} \widehat{SI}_i$ is the sum of SI estimates over all N_{SIC} SIC branches and $SI = \sum_{j=1}^{N_{SI}} SI_j$ is the actual SI signal influenced by all Tx-Rx coupled paths. Optimal performance can then be achieved by minimizing:

$$\begin{aligned} &argmin\, L\big(SI, \widehat{SI}\big) = argmin\, \tfrac{\sum(SI-\widehat{SI})^2}{nSamples} = \tfrac{1}{nSamples} \cdot \\ &\textstyle\sum_{n=1}^{nSamples} \Big(\sum_{j=1}^{N_{SI}} \alpha_j\big(x[n] \cdot \cos\theta_j - H\{x[n]\} \cdot \sin\theta_j\big) - \\ &\textstyle\sum_{i=1}^{N_{SIC}} \beta_i(x[n] \cdot \cos\vartheta_i - H\{x[n]\} \cdot \sin\vartheta_i)\Big)^2. \end{aligned} \quad (13)$$

With this relations parabolic characteristic the lowest value, where the value of cancellation signal approaches that of the interference, can be found at its mathematical vertex. Therefore, weighted parameters are iteratively updated as values converge towards the vertex:

$$\begin{aligned} \beta_i^{n+1} &= \beta_i^n + \eta \tfrac{\partial L}{\partial \beta_i^n} \\ \vartheta_i^{n+1} &= \vartheta_i^n + \eta \tfrac{\partial L}{\partial \vartheta_i^n}, \end{aligned} \quad (14)$$

In our simulation, the learning rate producing quickest convergence was heuristically determined and set as $\eta = 0.01$. A convergence mechanism was used where a targeted *convergence factor* was specified, denoting the percentage of reduction from initial loss needed to be achieved before the algorithm is considered to have converged adequately.

Variations of stochastic gradient descent (SGD) and mini-batch gradient descent (mini-BGD) were both evaluated; with the primary difference being the number of samples considered before parameter update. SGD, using a per-sample consideration, introduced more variation in updates but computationally proved easier at the cost of a slower rate of convergence. The other form, mini-BGD, computes the gradient using a small subset, or mini-batch, of the training data. This allows for potentially faster convergence.

2) SIC Performance Evaluation

Post training completion, each branch's weights retained their respective converged values in the simulated cancellation hardware. Ideally, these values permit perfect recreation of any interfering signal for antiphase nullification. However, inherent limitations prevent ideal convergence allowing for remaining residual SI to exist post cancellation. This performance of this imperfect

cancellation can then quantified via difference between the level of actual SI and residual SI.

This metric was realized by finding the decibel equivalence of the ratio of the remaining signal and power of the strongest IMD component envelope. An averaged moving-mean decibel ratio was then used to produce a single number indicative of overall SIC performance evaluation. This is described as follows:

$$SIC_{dBm} = 10\log_{10}\left(\frac{SI-\widehat{SI}}{0.001\cdot SI}\right). \quad (15)$$

Encapsulating performance in this way helps to provide a more comprehensive, simplistic picture of performance.

A summary of the overall simulation flowchart of the IBFD transceiver is shown in Fig. 3. The training of the analog SIC tap parameters with the gradient descent algorithm as well as the SIC performance measurement process are illustrated in the figure.

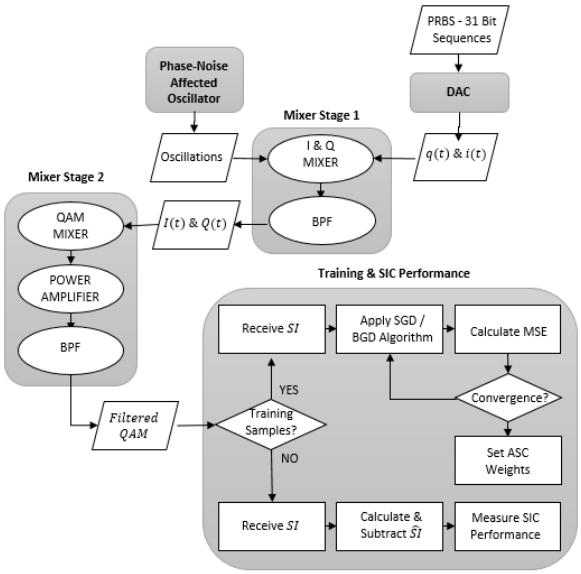

Figure 3. Simulation flowchart.

V. SIC Performance Evaluation Results

Results obtained are described in this section for the modelled transceiver utilizing IBFD technology that incorporates a real-time adjustable SI canceller operating in the analog domain. Emulated SIC hardware featured a Tx tapped four branch variable attenuation and phase shift control, where sampling location was selected to be immediately prior to the theoretical duplexing mechanism. The affective SI channel was emulated with 30 distinct theoretical paths, heuristically chosen, representing direct leakage, impedance discontinuity, and environmental reflection interference. In each simulation round, 5000 samples, from a total of 1,320,001 simulated samples, were selected to be used as training criteria for the SI canceller.

A. Stochastic v.s. Mini-Batch Gradient Descent

Initially, the simulations were performed to compare the performance of the SGD and mini-BGD algorithms employed in parameter setting of the canceller SIC. 200 simulations were equipartitioned at 50 runs each for SGD and mini-BGD with the latter's batch sizes of 10, 100, and 1000 samples. In Fig. 4 and Table IV the results can be seen juxtaposed for each partition's overall performance. The convergence factor discussed in Section IV-F was set to 0.01%. SGD results displayed the highest level of SIC achieved, averaging -60.1dB of cancellation. Compared with SGD, mini-BGD did not perform as well, with its SIC performance declining as the batch size increases. The worst performance was found in BGD-1000 (i.e., Mini-BGD, 1000 sample batch size) and exhibited a -29.6 dB mean interference cancellation.

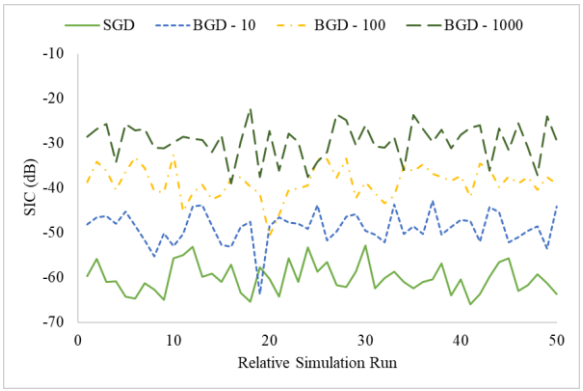

Figure 4. SIC performance of SGD and mini-BGD algorithms.

TABLE IV: SGD vs. Mini-BGD SIC Performance Comparison

Method	SIC Performance (dB)		Iterations
	Mean (μ)	*Deviation (σ)*	*Mean (μ)*
SGD	-60.1	3.31	6575
BGD-10	-48.9	3.60	6601
BGD-100	-38.7	3.53	6749
BGD-1000	-29.6	3.97	6503

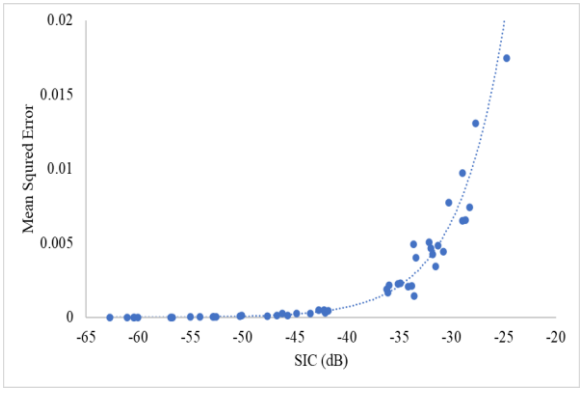

Figure 5. Effect of convergence factor on SIC performance

Table IV also includes the number of iterations required by each algorithm variant for weight updates until converge. The speed of convergence was only slightly different for SGD, BGD-10, and BGD-100. Among the four tested, BGD-1000 had the fastest convergence, although it was the overall worst performer, requiring 3.64% less iterative parameter updates than SGD.

In the following simulation runs, we decided to use only SGD to achieve the best SIC performance.

B. Effect of Convergence Factor

Convergence factor was the next variable simulation parameter that was evaluated for performance affect, with 100 SGD based runs being completed. Convergence factor was chosen from the values of {0.1%, 0.05%, 0.01%, 0.001, 0.0001%, 0.00001%}, while all other parameters were held fixed. A direct relationship between achieved MSE and convergence factor value was found. This relation showed that a smaller convergence factor yielded a smaller MSE. Fig. 5 plots the achieved SIC performance in dB versus the achieved MSE, providing a more accurate assessment of performance degradation. The trend shown by graphing the results reveal an exponential degradation in performance with increase in convergence factor.

We fixed the convergence factor to 0.0001% in the rest simulation runs to attain satisfactory SIC performance without significantly reducing convergence speed.

C. Effect of Noise and Nonlinearity

The next set of 100 simulation runs was used to evaluate the cancellation ability of the analog SIC against the self-interference corrupted by IMD products, harmonics, phase noise, and other systematic Gaussian noise. We further divided these simulations into two sets of 50 runs: one set served as the baseline, with only thermal noise and a small amount of phase noise affecting the system, and the other set was conducted with varying levels of distortion. For both sets, an SGD algorithm with a convergence factor of 0.0001% was used. All nonlinear distortion coefficients were selected from a uniform distribution U(0,1) and chosen randomly at that start of each simulation.

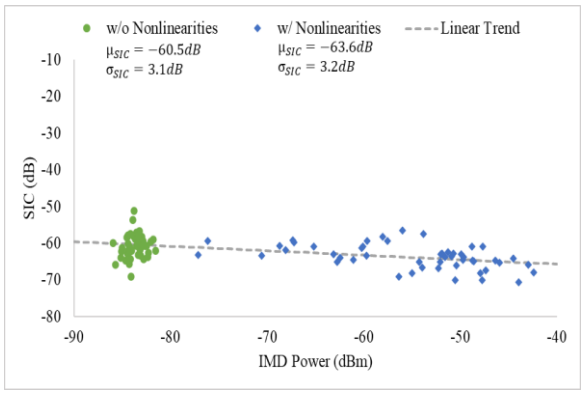

Figure. 6. Effect of transmission path distortion on SIC performance.

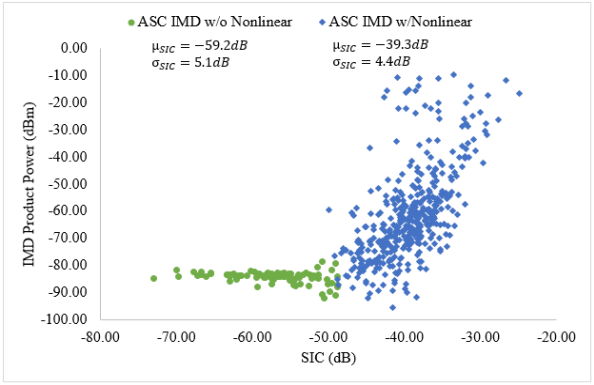

Figure 7. Effect of analog SIC nonlinearity on SIC performance.

The baseline simulations results in Fig. 6 shows an IMD product power level with an average of -83dBm. The achieved SIC levels are very close to the average value of -60.5dB with a standard deviation of 3.1dB. The noise-varying runs had IMD product levels ranging from approximately -78dBm to -42dBm. In these cases, the SIC performance are still close, with a mean SIC level of -63.6 dB with a standard deviation of 3.2dB. It seems that there was no direct correlation between the severity of the IMD products and the overall achieved SIC performance. Note that in the simulations the groups displayed performance that fell within one standard deviation with a linear trend line's slope of approximately -0.12dB.

D. Effect of Nonlinear Distortion in SIC Hardware

The goal of the last set of 500 simulation runs was to evaluate the impact of nonlinearity inherent to the canceller's hardware on overall cancellation performance. Similar to the practice in Section V-C, we divided simulations into two sets: The first 100 simulation runs were used as the baseline, with only thermal and phase noise included. The noise figure for the mixers was chosen randomly from U(4,14) and for the PA from U(2, 6). Additional nonlinear distortions were incorporated in the remaining 400 runs. A fifth order polynomial was chosen to model potential hardware nonlinearity that functionally was placed in-series with the canceller's input. The nonlinear coefficients of which were chosen randomly with a uniform distribution U(0,1). All simulations runs were performed using SGD with a convergence factor of 0.0001%.

Simulation results on the SIC performance of the IBFD transceiver in both simulation settings are included in Fig. 7. For the baseline scenario where in-series nonlinearity was not introduced, the power of IMD products was more constant with an average of -84.4dBm and a standard deviation of 2.1dBm. The achieved SIC level scattered around the mean of -59.2dB with a standard deviation of 5.1dB. The addition of nonlinear distortion caused the analog SIC to perform worse, with the average value reduced to -39.3dB with a standard deviation of 4.4dB. The degradation in SIC performance was approximately proportional to the power level of the IMD product. Specifically, the SIC performance degraded from approximately -50dB to -25dB as the IMD product power increased from -80dBm to -10dBm.

The decline in overall achieved SIC performance with stronger IMD product power suggests that unfavorable spectral content was added. The severity of the distortion's effect on the signal's spectrum did not prevent convergence during cancellation weight tuning. However, results showed that cancellation performance failed to yield improvement regardless of amplitude or phase adjustment. In other words, if the spectral content of the impinging SI was perfectly matched in both phase and amplitude values, the additional content induced in the cancellation hardware would be present in the residual SI. In effect, this intrinsic nonlinearity creates and forms another auxiliary path for SI incursion. Therefore, as the nonlinearity of the cancellation hardware becomes significant, cancellation performance can be expected to

proportionally degrade. This may be the phenomenon referred to in the IMD cost-balance relationship in Fig. 7.

We provide a mathematical explanation below for how nonlinear components in the SIC can cause performance degradation. For simplicity, imagine that a sinusoid signal in the form of $\cos\omega t$ is transmitted. The analog SIC receives a portion of this signal's energy, which can be represented as $a_1\cos\omega_1 t$. If we assume that the SIC has a basic 2nd-order polynomial model, then the spectral content of the cancellation signal is represented by $a_2\cos\omega_1 t + \frac{a_2^2}{2}\cos 2\omega_1 t + \frac{a_2^2}{2}$. Next, we allow the nonlinear signal in our SIC to be manipulated by any amplitude and phase changes with weights a_w and θ_w, the cancellation signal becomes

$$a_w a_2\cos(\omega_1 t + \theta_w) + \frac{a_w a_2^2}{2}\cos(2\omega_1 t + \theta_w) + \frac{a_w a_2^2}{2}. \quad (16)$$

Similarly, the incoming SI is varied from the original transmitted signal with amplitude and phase manipulations. Let a_{SI} and θ_{SI} denote the respective attenuated amplitude and phase shift of a single path SI component, respectively, the SI signal in this path becomes $a_{SI}\cos(\omega t + \theta_{SI})$. Then, the achievable cancellation of the two signal becomes:

$$a_{SI}\cos(\omega_1 t + \theta_{SI}) - \left[a_w a_2\cos(\omega_1 t + \theta_w) + \frac{a_w a_2^2}{2}\cos(2\omega_1 t + \theta_w) + \frac{a_w a_2^2}{2}\right]. \quad (17)$$

To make this easier to understand, we simplify this example further and assume the phases are matched perfectly and equal to 0 (i.e., $\theta_{SI} = \theta_w = 0$). Since the value of the input signal a_1 is unknown and could theoretically take any value, we can arbitrarily set a_2 to 1 for simplicity. As a result, now our possible cancellation in (17) becomes:

$$a_{SI}\cos(\omega_1 t) - \left[a_w\cos(\omega_1 t) + \frac{a_w}{2}\cos(2\omega_1 t) + \frac{a_w}{2}\right]. \quad (18)$$

It is clear from (18) that perfect cancellation occurs only when the SIC output (i.e., the bracketed terms) matches the SI component. We can graphically solve this by checking the intersections of the two components when $\omega_1 t$ ranges from 0 to 2π, and allowing a_w and a_{SI} to take on various possible values. Unless $a_w = a_{SI} = 0$, it is clear that at most four points exist where perfect cancellation could be achieved. At these specific times, SIC degradation does not occur. However, at all other times, the nonlinear components in the SIC will cause its performance to degrade. Therefore, it is almost inevitable that the SIC hardware will cause performance degradation, and mitigating this impact is non-trivial.

VI. Discussions and Future Work

The in-band full-duplex assumption has been demonstrated in various theoretical simulations and one-off ad-hoc prototypes, but to the best of our knowledge, there has been no production-ready IBFD transceiver created yet. Traditionally, such development has been prevented by the challenge of providing sufficient transmitter-to-receiver isolation from disproportionately large amounts of self-interference. Nevertheless, recent advances in SIC techniques have shown that, when properly deployed, they provide a means to combat this serious offender. To enhance the cancellation capability, multiple SIC mechanisms should be used together across different domains. To prevent and suppress interference in the propagation domain, techniques such as high isolation duplexers, circulators, and antenna-nulling methods should be used. As demonstrated in this paper, the next and first line of defense against Tx-Rx coupled interference is the responsibility of analog domain cancellation, the overall performance of which largely determines the effectiveness of the IBFD transceiver. Subsequent digital domain techniques that exploit the transceiver's foreknowledge may be useful for residual self-interference cleanup.

In this paper, we extend our prior work in [24] to evaluate the analog self-interference cancellation performance for IBFD wireless communication. We implemented a 512QAM IBFD transceiver model in MATALB and evaluated its analog SIC performance. This transceiver architecture was shown to be able to achieve up to and beyond 60dB of aggregate cancellation through the inclusion of a variable amplitude and phase branched canceller that samples the signal after primary distortions have occurred. It is noteworthy that no additional circuitry or channel modeling was necessary to account for nonlinear distortion. However, the ability of the cancellation hardware to effectively cancel nonlinear distortion is dependent on its own level of nonlinearity. If this level is significant and not properly accounted for, the overall cancellation may be greatly reduced in efficacy. Additionally, because this technique involves tapping a signal as close to the RF frontend as possible, it is likely that higher power signals will be encountered. In practice, the primary tools for sampling these high-power signals are baluns or directional couplers, which are known to produce intermodulation distortion at higher powers. Even after that, nonlinearity is difficult to avoid in any device that attempts to manipulate signal phase, delay, or magnitude. However, the exact degree and impact of this nonlinearity have yet to be determined.

It is worth mentioning that caution should be exercised when considering the reported values for this model. By definition, a model is an estimated depiction of an observed phenomenon. Therefore, any model will inherently have assumptions and limitations that impact its overall accuracy. For instance, although this model allowed for any possible phase or magnitude variation in a stochastic fashion when generating the SI channel, it did not account for the actual propagation time delay. If the self-interference is limited to direct leakage and antenna mismatch, then this time delay may be insignificant due to the signal's propagation velocity. However, as the contribution of reflection paths becomes more significant (e.g., in outdoor environments or larger arenas), the estimated SI channel may no longer accurately reflect the actual conditions. Further research on the propagation patterns of 2.4GHz and 5GHz signals in various settings could improve the ability of the model to estimate and incorporate delayed channel characteristics. Another

suggestion for future work is to incorporate a dynamic SI channel model to evaluate the overall negative impact and potentially identify methods for improvement.

Other potential future work includes extending this model to include digital cancellation techniques. Because the effectiveness of digital cancellation is directly dependent on the overall analog cancellation, expanding the model to include digital cancellation would allow for a better understanding of the interaction between the two and could reveal which nonlinear or noise sources are most difficult to mitigate and any constraints on the efficacy of digital cancellation. Furthermore, expanding this study to include MIMO systems could provide insight into the viability of the tapped-branch architecture in comparison to the anticipated increase in circuit complexity.

Conflict of Interest

The authors declare no conflict of interest.

Author Contributions

Both authors contributed to the paper through regular discussions and revisions. Jonathan Shilling and Chao Chen formulated the idea and system framework. Jonathan Shilling developed the system model, conducted experiments, and summarized results. Chao Chen revised and reviewed the content of the paper. Both authors approved the final version of the paper.

References

[1] A. Goldsmith, *Wireless Communication*, Cambridge Univ. Press, 2005.

[2] A. Sabharwal, P. Schniter, D. Guo, D. W. Bliss, S. Rangarajan, and R. Wichman, "In-band full-duplex wireless: Challenges and opportunities," *IEEE Journal on Selected Areas in Communications*, vol. 32, no. 9, pp. 1637–1652, Sept. 2014.

[3] D. Kim, H. Lee, and D. Hong, "A survey of in-band full-duplex transmission: From the perspective of phy and mac layers," *IEEE Communications Surveys & Tutorials*, vol. 17, no. 4, pp. 2017–2046, 2015.

[4] Z. Zhang, K. Long, A. V. Vasilakos, and L. Hanzo, "Full-duplex wireless communications: Challenges, solutions, and future research directions," in *Proc. IEEE*, vol. 104, no. 7, pp. 1369–1409, July 2016.

[5] H. B. Salameh, Z. Khader, and A. Al Ajlouni, "Intelligent secure networking in in-band full-duplex dynamic access networks: Spectrum management and routing protocol," *Journal of Network and Systems Management*, vol. 29, no. 2, Apirl. 2021.

[6] K. Pärlin and T. Riihonen, "Full-duplex transceivers for defense and security applications," *Full-Duplex Communications for Future Wireless Networks*, pp. 249–274, Springer, 2020.

[7] K. A. Darabkh, O. M. Amro, H. B. Salameh, and R. G. Al-Zubi, "A–Z overview of the in-band full-duplex cognitive radio networks," *Computer Communications*, vol. 145, Sept. 2019, pp. 66-95.

[8] J. I. Choi, M. Jain, K. Srinivasan, P. Levis, and S. Katti, "Achieving single channel, full duplex wireless communications," in *Proc. ACM MobiCom*, Chicago, IL, USA, Sept. 2010, pp. 1-12.

[9] M. Duarte and A. Sabharwal, "Full-duplex wireless communications using off-the-shelf radios: Feasibility and first results," in *Proc. 2010 Conference Record of the Forty Fourth Asilomar Conference on Signals, Systems and Computers*, 2010, pp. 1558-1562.

[10] D. Bharadia, E. Mcmilin, and S. Katti, "Full duplex radios," *ACM SIGCOMM Computer Communication Review*, vol. 43, October 2013, pp. 375-386.

[11] T. Vial, A. Lefevre, M. L. Penven, and Q. Bodinier, "A short review of current challenges and potential applications of full duplex in wireless networks," in *Proc. 2017 XXXIInd General Assembly and Scientific Symposium of the International Union of Radio Science*, 2017, pp. 1-4.

[12] C. Despina-Stoian, A. Digulescu-Popescu, S. Alexandra, R. Youssef, and E. Radoi, "Comparison of adaptive filtering strategies for self-interference cancellation in LTE communication systems," in *Proc. 13th International Conference on Communications (COMM)*, 2020, pp. 73-76.

[13] K. E. Kolodziej, B. T. Perry, and J. S. Heed, "In-band full-duplex technology: Techniques and system survey," *IEEE Trans. on Microwave Theory and Techniques*, vol. 67, no. 7, pp. 3025- 3041, July 2019.

[14] S. Sadjina, C. Motz, T. Paireder, M. Humer, and H. Pretl, "A survey of self-interference in LTE-advanced and 5G new radio wireless transceivers," *IEEE Trans. on Microwave Theory and Techniques*, vol. 68, no. 3, pp. 1118-1131, March 2020.

[15] C. D. Nwankwo, L. Zhang, A. Quddus, M. A. Imran, R. Tafazolli, "A survey of self-interference management techniques for single frequency full duplex systems," *IEEE Access*, vol. 6, pp. 30242-30268, 2018.

[16] L. Song, R. Wichman, Y. Li, and Z. Han, *Full-duplex Communications and Networks*. Cambridge, United Kingdom: Cambridge University Press, 2017.

[17] N. Singh, D. Gunawardena, A. Proutiere, B. Radunovi, H. V. Balan, and P. Key, "Efficient and fair MAC for wireless networks with self-interference cancellation," in *Proc. 2011 International Symposium of Modeling and Optimization of Mobile, Ad Hoc, and Wireless Networks*, 2011, pp. 94-101.

[18] M. A. Alim, M. Kobayashi, S. Saruwatari, and T. Watanabe, "In-band full-duplex medium access control design for heterogeneous wireless LAN," *EURASIP Journal on Wireless Communications and Networking*, 2017, Article number: 83 (2017).

[19] M. E. Dieckmann, A. Ynnerman, S. C. Chapman, G. Rowlands, and N. Andersson, "Simulating thermal noise," *Physica Scripta*, vol. 69, no. 6, pp. 456–460, 2004.

[20] H. Nyquist, "Thermal agitation of electric charge in conductors," *Physical Review*, vol. 32, no. 1, pp. 110–113, 1928.

[21] M. Isaksson, D. Wisell, and D. Ronnow, "A comparative analysis of behavioral models for RF Power Amplifiers," *IEEE Transactions on Microwave Theory and Techniques*, vol. 54, no. 1, pp. 348–359, 2006.

[22] T. Fukui, K. Komatsu, Y. Miyaji, and H. Uehara, "Analog self-interference cancellation using auxiliary transmitter considering IQ imbalance and amplifier nonlinearity," *IEEE Trans. on Wireless Communications*, vol. 19, no. 11, pp. 7439–7452, Nov. 2020.

[23] J. Watt, R. Borhani, and A. K. Katsaggelos, *Machine Learning Refined: Foundations, Algorithms, and Applications*, Cambridge, United Kingdom: Cambridge University Press, 2020.

[24] J. Shilling and C. Chen, "Impact of noise and nonlinearity on analog self-interference cancellation in in-band full-duplex communications," in *Proc. 11th International Conference on Communications, Circuits and Systems (ICCCAS 2022)*, pp. 75-82, Singapore, 2022, pp. 75-82.